The Effects Of Battery Initial State Of Charge On The Energy Distribution Of Vehicles Under WLTC Driving Cycle

Jie Zhang[1*], Xiaobing Wu[2], Hongwei Guo[1], and Tao Wu[3]

[1] School of Automobile, Zhejiang Institute of Communications, Hangzhou 311112, China
[2] Zhejiang Technology Innovation Service Center, Hangzhou 310007, China
[3] School of Mechanical and Automotive Engineering, Shanghai University of Engineering Science, Shanghai 201620, China
[*] Corresponding author. E-mail: Jerry9788@126.com

Received March 13, 2026; accepted August 1, 2026

During vehicle operation, the initial state of charge (ISOC) of the onboard battery affects the control strategies governing battery and generator operation, which in turn influences the vehicle’ s energy distribution. In this study, an SUV equipped with an intelligent start-stop system and braking energy recovery was tested on a chassis dynamometer under the worldwide harmonized light vehicles test cycle (WLTC) to investigate the effects of three battery ISOC levels – 45%, 70% (battery threshold), and 85% – on vehicle energy distribution. The results show that ISOC exerts a significant influence on battery and generator operation, thereby affecting energy recovery efficiency. A battery ISOC of 85% favors improved vehicle energy efficiency and reduced fuel consumption. Conversely, at an ISOC of 45%, the vehicle exhibits the highest fuel consumption, an increase of more than 8%, indicating that operation with an ISOC substantially below the threshold should be avoided. This study develops a practical experimental method that links the easily measurable ISOC parameter to holistic vehicle energy performance, offering a novel and efficient approach to indirectly evaluate how gradual battery degradation affects vehicle fuel economy without the need for long-term aging tests.

Keywords: initial state of charge; battery; energy distribution; energy recovery; WLTC

http://dx.doi.org/10.6180/jase.202611_34.036

1. Introduction

Currently, to alleviate carbon dioxide emissions and reduce petroleum resources consumption in the transportation field, battery electric vehicles (BEVs) and hybrid electric vehicles (HEVs) have developed vigorously. Nevertheless, internal combustion engine (ICE) vehicles, namely fuel-powered vehicles, are anticipated to persist as the predominant powertrain for the foreseeable decades [1].Consequently, enhancing the energy efficiency and reducing fuel consumption of fuel-powered vehicles remains of great practical importance.

The state of charge (SOC) of onboard batteries is typically defined as the ratio of the current remaining capacity to the rated capacity, which intuitively reflects the remaining power of the battery [2]. SOC serves as the fundamental basis and core parameter for vehicle energy distribution and dynamic power coordination. It is not only an intuitive indicator of the energy state for electric vehicles, but also a core parameter underpinning vehicle energy management, battery safety protection, lifespan prediction and control strategy optimization [3]. Accurate and real-time SOC estimation is critical for improving the overall energy efficiency of BEV and HEV, ensuring system safety, optimizing user experience and diminishing the total lifecycle cost [4, 5]. In HEVs, SOC planning and tracking directly govern the power distribution between the engine and the motor, with the objectives of minimizing equivalent fuel consumption or satisfying pure electric driving requirements in designated zones (e.g. zero-emission zones) [6, 7]. Previous studies have pointed out that SOC trajectory optimization markedly enhances system energy efficiency and reduces energy consumption. And its accuracy is a prerequisite for the practical implementation of theoretically optimal control methods such as dynamic programming and model predictive control [8, 9]. Fuel cell hybrid electric vehicles(FCHEVs) typically employ a hybrid powertrain topology comprising fuel cells and auxiliary energy storage devices (power batteries or supercapacitors) [10]. In this configuration, SOC, as a critical state parameter characterizing the instantaneous energy of the energy storage system, directly determines the dynamic power distribution between fuel cells and batteries [11]. Research has demonstrated that the equivalent consumption minimization strategy (ECMS) or fuzzy logic control strategies based on SOC feedback can effectively regulate the power output of both sources, ensuring that the power battery operates within its high-efficiency SOC range, thereby avoiding efficiency losses caused by overcharging or over-discharging [12, 13]. Consequently, SOC-based ECMS control strategies are most frequently applied in the context of FCHEVs.

In conventional fuel-powered vehicles, lead-acid batteries, as crucial components within the power supply system, undertake auxiliary power supply duties for engine starting, vehicle lighting, infotainment systems, and various electronic control units [14]. As vehicle electrification and intelligence progress, the onboard electrical loads have increased sharply, imposing more stringent demands on battery management [15, 16]. Starting the engine in fuel vehicles requires the battery to deliver a substantial instantaneous current. The SOC value is directly correlated with the battery's cranking power capability, and a low SOC state frequently leads to excessively low cold start voltage and causes starting failure [17]. Through accurate SOC monitoring, the power management system can assess whether the available energy is sufficient to support the next engine start, particularly in micro-hybrid vehicles equipped with intelligent start-stop systems [18]. These systems require continuous SOC monitoring during engine shutdown to ascertain whether automatic shutdown is permissible, thereby preventing vehicle restart failure due to insufficient energy [19].

Modern fuel-powered vehicles are generally outfitted with generators featuring intelligent charging strategies [20, 21]. Battery SOC serves as a critical input for regulating generator charging and battery discharging [22]. The power management system establishes hierarchical energy levels according to the SOC state monitored by the battery sensor [23]. At a high SOC, the system can appropriately reduce the generator output voltage or disconnect non-essential loads, using the battery for auxiliary power supply to reduce engine mechanical loss. Conversely, at a low SOC, the system increases generator output or restricts comfort loads, such as infotainment systems, to prioritize battery charging. This dynamic balance process relies entirely on real-time SOC feedback. Several studies have confirmed that the fuel consumption of fuel vehicles can be effectively reduced by optimizing the battery SOC control strategies [24, 25]. For example, during vehicle deceleration and coasting, the system enables the generator to raise its voltage for energy recovery when the SOC is low. When the SOC is sufficient, unnecessary power generation is avoided, thereby lowering engine load. Overcharging and over-discharging are major contributors to lead–acid battery lifetime degradation. Maintaining SOC within a reasonable window can effectively suppress battery sulfation caused by deep discharge or water loss from overcharging, thus extending service life [26].

In summary, extensive research has been conducted on SOC estimation for BEVs and HEVs [27, 28]. Kim et al. [29] studied the effects of the battery ISOC on tractive propulsion characteristics of an HEV. They find that the ISOC leads to significant disparities in the electric current balance during hybrid operation mode, necessitating meticulous coordination between the ICE and motor to ensure adequate vehicle propulsion capacity while maintaining the battery SOC at a reasonable level. However, research specifically addressing the battery initial state of charge (ISOC), a deterministic starting condition influenced by parking periods and battery health, remains sparse for conventional fuel vehicles. More critically, while the importance of SOC is acknowledged, the quantitative impact of ISOC variations on the real-time energy distribution, and specifically on the efficiency of advanced features like braking energy recuperation in modern intelligent fuel vehicles, is yet to be systematically investigated and empirically quantified. Vehicles equipped with intelligent start-stop and braking energy recovery systems, are particularly worthy of in-depth investigation. Against this background, the primary objective of this study is to conduct a detailed, quantitative analysis of the effects of battery ISOC on energy distribution and fuel consumption of a modern fuel vehicle, equipped with intelligent start-stop and braking energy recovery systems, under the worldwide harmonized light vehicles test cycle (WLTC), The main purpose of current work aims to investigate the impact of battery ISOC degradation, stemming from battery aging or failure, on energy distribution. To achieve this, a practical experimental framework was established, where the readily measurable ISOC parameter is directly linked to whole-vehicle energy performance

Table 1. Main test equipment.

Equipment	Model	Manufacturer	Accuracy
Chassis dynamometer	VULCAN II EMS-CD48L	HORIBA	±0.005% f.s.
Power analyzer	PW3390	HIOKI	±0.05% f.s.
Current clamp	CT6844-05	HIOKI	±0.02% f.s.
Onboard fuel meter	AVL KMA Mobile	AVL List	±0.5%

metrics. The novelty of this study lies in quantitatively revealing the effects of battery ISOC variation on the energy distribution of a specific fuel vehicle equipped with intelligent start-stop and regenerative braking systems. The findings expand the research methodologies and database concerning battery ISOC effects on energy distribution in ICE vehicles. The approach proposed in this study provides a novel perspective for indirectly assessing the impact of gradual battery degradation on vehicle-level fuel economy without long-term aging tests.

2. Experiment setup and methods

2.1. Experiment setup

The test vehicle is a midsize SUV powered by a 2.0T gasoline direct-injection (GDI) engine, fitted with a 12 V lead-acid battery with a capacity of 58 A· h. Fig. 1 shows a schematic diagram of the energy flow topology of the test vehicle. During vehicle operation, energy distribution is realized as the engine converts thermal energy from fuel combustion into mechanical energy. A portion of this energy supplies the kinetic energy required for vehicle propulsion. Another portion drives the generator via the engine to produce electrical energy to power onboard electrical equipment. The vehicle incorporates a braking energy recovery function. During deceleration or braking, kinetic energy is recovered and converted into electrical energy via the generator to charge the battery. The vehicle also features an intelligent start-stop function. When the battery SOC is below 60%, the start-stop function is deactivated, and the engine continues to idle. When the battery SOC exceeds 60%, the function is reactivated, and the engine shuts off during idle periods.

This test was carried out on a chassis dynamometer, and the main test equipment is listed in Table 1. A power analyzer was used to measure battery voltage, and a current clamp was used to measure battery current. An onboard fuel consumption meter measures vehicle fuel consumption. Key state parameters such as battery SOC temperature, generator current, voltage and temperature were acquired via the vehicle OBD (onboard diagnosis) interface. To minimize the influence of ambient temperature, the laboratory temperature was controlled at 25 °C.

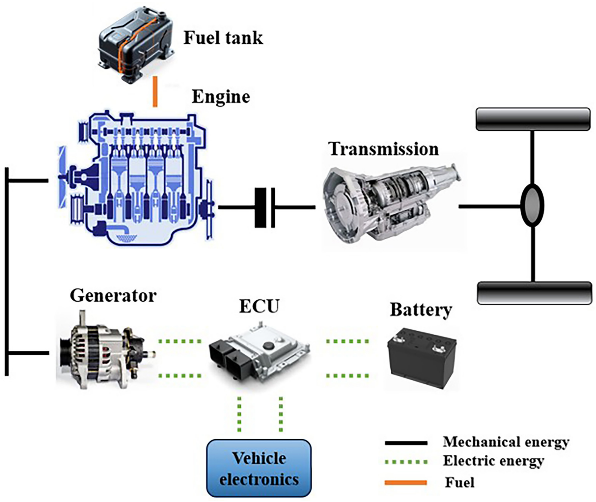

Fig. 1. Schematic diagram of energy flow topology of the test vehicle

Table 2. Main physical and chemical properties of test gasoline.

Fuel Type	95# Gasoline
RON	96.5
Density (20°C)	740.6 kg/m^3
Lower Heating Value	42.58 MJ/kg
H Content	84.64 (m/m) %
C Content	13.15 (m/m) %

The test vehicle used commercially available 95# gasoline in China, with a research octane number (RON) of no less than 95. Its detailed physical and chemical properties are presented in Table 2.

2.2. Test Methods

In this study, the vehicle was tested on a chassis dynamometer following the WLTC driving cycle [30], illustrated in Fig. 2. The WLTC is the global core standard for light-duty vehicle energy consumption evaluation, with a total duration of 1800 s and a total mileage of 23.266 km, and a prescribed vehicle speed for each second. The full WLTC cycle is divided into 4 speed phases: low speed, medium speed, high speed and extra-high speed, each with specified duration and distance (see Table 3).

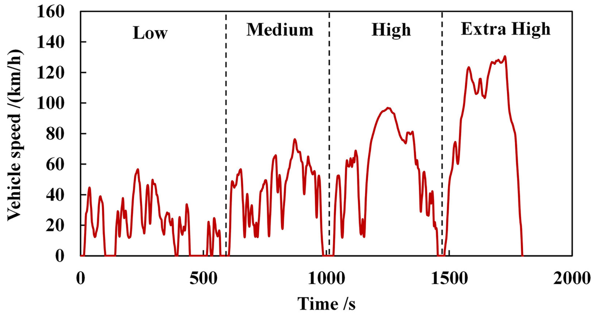

Fig. 2. WTLC driving cycle

Table 3. Time and mileage of each speed segment in WLTC.

Speed Segment	Time/s	Mileage/km
Low Speed	589	3.095
Medium Speed	433	4.756
High Speed	455	7.162
Extra-High Speed	323	8.254
Total	1800	23.266

Under the WLTC cycle, the energy generated by the generator may originate from fuel combustion or braking energy recovery conditions. To identify operating conditions under which generator power corresponds to energy recovery, raw WLTC data were processed according to the process shown in Fig. 3. Five conditions were derived from the calibrated braking energy recovery control strategy of the test vehicle.

When the vehicle gear selector is in D drive position, and the vehicle remains in forward motion or stationary, the condition is expressed as Eq. (1):

$$D = \begin{cases} 1, & \text{D position} \\ 0, & \text{otherwise} \end{cases} \tag{1}$$

When engine speed N_{eng} exceeds 1000 rpm, the condition is expressed as Eq. (2):

$$N_{\text{eng}} > 1000\,\text{rpm} \tag{2}$$

When the engine is in fuel-cutoff mode, the fuel-cutoff control signal S_{fuel} equals 1, as shown in Eq. (3):

$$S_{\text{fuel}} = \begin{cases} 1, & \text{cutting-off fuel} \\ 0, & \text{otherwise} \end{cases} \tag{3}$$

When the battery current is in charging mode and current is positive, the condition is expressed as Eq. (4):

$$I_{\text{bat}} > 0\,\text{A} \tag{4}$$

When the battery is charging and SOC exceeds the threshold (70% in this study), the expression is expressed as Eq. (5):

$$\text{SOC} > 70\% \tag{5}$$

When all five conditions are satisfied, the operation state is classified as energy recovery, as shown in Eq. (6). Concurrently, data including time, current, and energy were recorded and statistically analyzed. Otherwise, the condition is not categorized as energy recovery.

$$f(D, N_{\text{eng}}, S_{\text{fuel}}, I_{\text{bat}}, \text{SOC}) = \begin{cases} \text{Energy recovery data,} & D = 1 \wedge N_{\text{eng}} > 1000 \wedge S_{\text{fuel}} = 1 \\ & \wedge\, I_{\text{bat}} > 0 \wedge \text{SOC} > 70\% \\ \text{Non energy recovery data,} & \text{otherwise} \end{cases} \tag{6}$$

The test vehicle was a commercially available model, so its control strategy is fixed. However, the control strategies vary among different car manufacturers or models, which directly affects the energy and efficiency of braking energy recovery. Based on this process, the energy recovery data of three ISOC levels were processed.

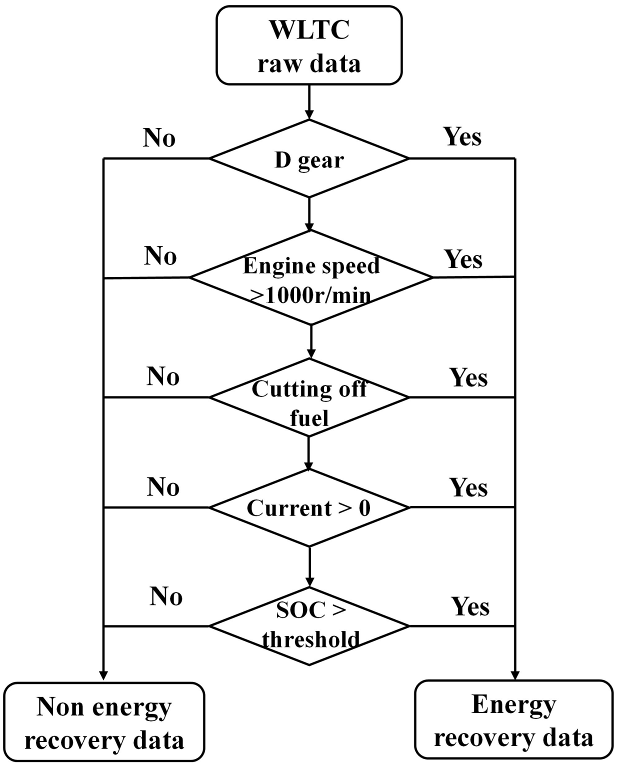

Fig. 3. Energy recovery condition judgment process.

Battery SOC threshold is a critical parameter for energy flow control, which governs the operating modes of the battery and generator. Although advanced SOC control methods, such as model predictive control (MPC), are available, this study focuses primarily on the impact of ISOC on energy distribution. To eliminate interference from other factors, a manual SOC threshold setting method was adopted, which facilitates targeted experimental analysis. In this study, the battery charging-discharging SOC threshold was set to 70%. When battery SOC is less than 70%, the generator charges the battery. While the SOC is greater than 70%, the battery discharges to power vehicle electrical equipment. Although battery SOC is a dynamic parameter, the 70% threshold was selected as the equilibrium point to regulate vehicle energy flow. This setup enables the battery to maintain continuous power balance during operation and restricts large SOC fluctuations.

To investigate the effects of different battery ISOC levels on vehicle energy distribution, three test rounds were performed over the full 1800s WLTC cycle. Each test was repeated twice, and the average value was taken. ISOC levels of 45%, 70%, and 85% were selected to represent three typical states of ISOC implementation in real-world vehicle operation. Among them, 70% corresponds to the calibrated charge-discharge threshold of the test vehicle battery. 45% is a representative sub-threshold value. Similarly, 85% is a representative super-threshold value. Second-by-second transient data of key battery and generator state parameters were recorded at ISOC of 45%, 70% and 85%, including battery current, voltage, temperature and SOC, and generator current, voltage and temperature. Simultaneously, full WLTC cycle data were statistically analyzed, calculated, and compared, covering total battery charge–discharge duration, generator operating duration, energy recovery duration, average battery charge–discharge current, average generator output current, average energy recovery generator current, battery charge–discharge energy, generator energy, onboard electrical load energy, recovered energy, and energy recovery efficiency.

3. Results and discussion

3.1. WLTC transient test results

Based on the full 1800 s WLTC test cycle, the instantaneous characteristics of battery and generator performance and state parameters were measured at battery ISOC levels of 45%, 70% and 85%.

3.1.1. Battery ISOC=45%

Fig. 4 illustrates the transient characteristics of both battery and generator performance along with their state parameters throughout the full WLTC cycle at an ISOC = 45%. Specifically, Fig. 4(a) shows battery current, voltage, SOC and temperature, while Fig. 4(b) presents the generator output current, voltage and temperature. It can be observed that the battery SOC remains below the 70% threshold throughout the WLTC cycle, primarily due to the excessively low ISOC value (only 45%). In the battery current diagram, positive values denote charging whereas negative values indicate discharging. The maximum charging current is 17 A, and the maximum discharging current reaches-295 A. The peak battery voltage is 14.1 V, while the minimum voltage drops to 10.1 V. During the initial 1240seconds, the battery maintains a continuous charging mode with a constant current of approximately 30 A and a stable voltage of 13 V. At 1240 s, when the battery SOC rising to 60%, the generator current increases to 120 A and voltage rises to 14.8 V. Accordingly, battery current and voltage also rise, with the current reaching 75 A and the voltage climbing to 14.1 V. The battery temperature gradually increases with operating time, ranging from 26 °C to 48 °C. After more than 1000 seconds of charging and when the SOC = 55%, the temperature rising rate accelerates. After 1600 s the temperature stabilizes at 48 °C. Meanwhile, the generator temperature rises from 28 °C to 112 °C.

3.1.2. Battery ISOC=70%

The transient characteristics of the battery and generator performance and state parameters at ISOC =70% are illustrated in Fig. 5. During testing, the battery SOC maintains an equilibrium state with minor fluctuations around the threshold of 70%. Over the 1800 s WLTC test, the battery current remains between -1 A and 1 A (near 0 A) for approximately 200 s. This indicates that the vehicle operates in an electrical equilibrium state where the generator supplies power directly to onboard electrical appliances. The maximum battery charging and discharging currents are 77 A and -361 A respectively. The maximum voltage reaches 14.7 V, while the minimum voltage is 10.6 V. The peak generator current is 123.6 A, and the minimum voltage is 8.8 V, while the maximum voltage is 15.1 V. The battery temperature gradually rises with operating time, from 26 °C to 40 °C, and stabilizes after 1600 s. Generator temperature increases from 28 °C to 92 °C. At the threshold ISOC of 70%, the generator load demand is reduced by about 13% compared to the ISOC of 45% condition The current is lowered by 0.9 A, resulting in a lower peak temperature.

3.1.3. Battery ISOC=85%

Fig. 6 presents the performance and state parameter curves of the battery and generator over the full WLTC cycle at ISOC =85%. Since the ISOC exceeds the 70% threshold, the battery spends more time in discharging mode, and SOC decreases to the threshold of 70% by the end of the

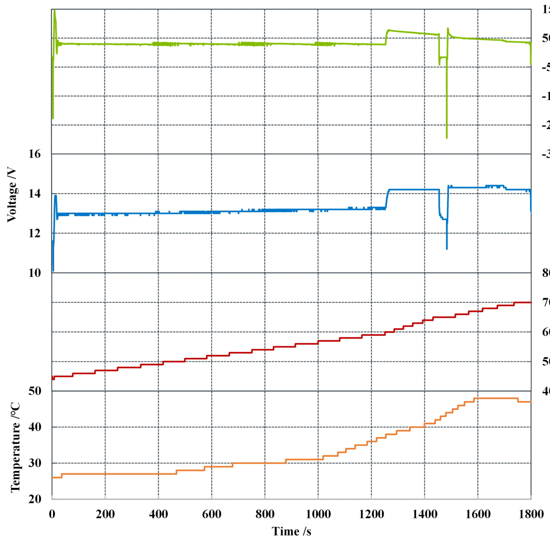

(a) Battery

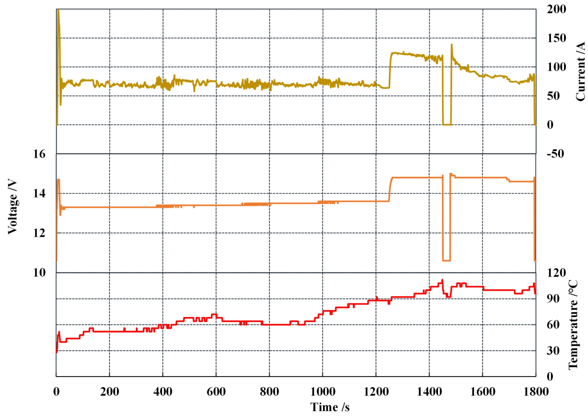

(b) Generator

Fig. 4. Instantaneous characteristics of battery and generator parameters at ISOC=45%.

(a) Battery

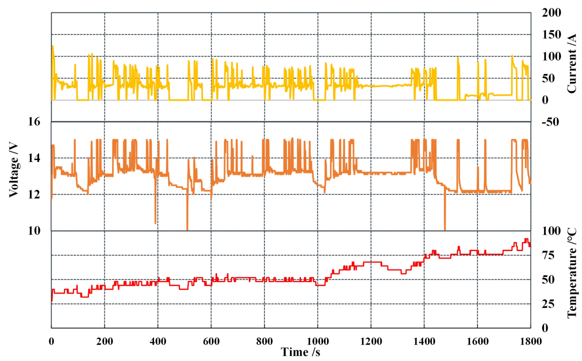

(b) Generator

Fig. 5. Instantaneous characteristics of battery and generator parameters at ISOC=70%.

test. Under WLTC engine-off conditions, the generator also ceases operation. However, the battery sustains onboard electrical appliances, with the current mostly maintained at -15 A and voltage at the rated 12 V. During vehicle starting, the starter motor draws battery current exceeding -300 A, and battery voltage drops by 1 V-2 V.

Under the WLTC cycle, the maximum battery current is 135 A and the peak voltage achieves 14.6 V. During the generator operation, the maximum voltage is 15.1 V and the maximum current reaches 168 A, which is a transient peak. The generator specifications installed on the test vehicle allow for a short-term peak output current of 180 A with a duration of 30 seconds. The battery temperature gradually increases with operating time, from 25 °C to 37 °C. Accordingly, generator temperature rises from 28 °C to 84 °C.

By combining Figs. 4 - 6, it is evident that the peak temperatures of both the battery and generator decrease as ISOC increases. For instance, when the ISOC increases from 45% to 70% and 85%, battery peak temperature drops from 48 °C to 40 °C and 37 °C, respectively. Simultaneously, the generator peak temperature decreases from 112 °C to 92 °C and 84 °C. Therefore, a high ISOC helps reduce the maximum operating temperature of the battery and generator, thereby promoting high-efficiency operation and extended service life.

3.2. WLTC test statistical results

A comparison of the battery and generator operating durations under the three ISOC states is shown in Fig. 7. It can be seen that the operation duration of each module is strongly correlated with the ISOC value, and the vehicle control system takes ISOC as a key parameter to allocate the action time of each module. At ISOC = 45%, both the battery charging duration and the generator operating duration are very long, exceeding 1700 s, meaning near-continuous operation throughout the full WLTC cycle. When ISOC is set to 70%, the generator operates for 1451 seconds, and battery charging and discharging durations are relatively close. When ISOC equals 85%, the generator operating duration is significantly reduced, while battery discharging duration is relatively long (1532 s) and charging duration is only 268 s. This indicates that a high ISOC corresponds to a shorter energy recovery duration.

A comparison of average battery and generator currents in the WLTC cycle under varying ISOC levels is presented in Fig. 8. When ISOC is 45%, the generator operates continuously, with an average current of 79 A, the highest among the three conditions. The energy recovery current is also high, but the average battery charging current is only 37 A, mainly because a large portion of the current is consumed by onboard electronic components consume. At ISOC = 70%, all average current values are the lowest. This indicates that small current fluctuations across electrical components and stable SOC maintenance at the threshold. When ISOC equals 85%, the average currents of battery charging and energy recovery are high, suggesting elevated component operating currents to facilitate rapid battery discharging. However, the average generator current and average battery discharging current are close to those at an ISOC of 70%.

A detailed energy comparison of each component across the three ISOC states is displayed in Fig. 9. When ISOC stands at 45%, the generator operates continuously at a high current, yielding substantial generator output energy and charging energy. Prolonged engine operation (e.g., ignition coil, oil pump, etc.) also leads to high electrical energy consumption. The recovered energy registers at 35 W·h, a medium level, while the discharged energy is nearly negligible. At an ISOC of 70%, all generator energy is consumed by onboard electrical appliances, and battery energy remains nearly unchanged from the start to the end of the WLTC cycle (refer to Fig. 5(a)), with the least recovered energy. This attributes to low generator operating current, the small difference between charging and discharging energy, and a stable battery SOC. When ISOC climbs to 85%, surpassing the threshold, battery discharging energy inevitably rises, whereas generator energy, battery charging and electrical load energy are low. Recovered energy is the highest among the three conditions, mainly due to the high operating current of the generator.

Table 4 serves as a supplementary counterpart to Fig. 9, providing a quantitative breakdown of the proportion of each energy source relative to the total fuel energy consumption. As illustrated in the table, the proportion of engine energy exhibits a consistent downward trend. Whereas the share of discharge energy rises steadily, demonstrating a distinct negative correlation between these two energy sources. This trend can be explained by variations in ISOC: a higher ISOC corresponds to a greater remaining battery capacity. Under such circumstances, the system primarily relies on battery discharge for power supply, reducing the direct fuel energy consumption of the engine. As a result, the overall energy utilization efficiency improves, and fuel consumption is effectively lowered.

Additionally, both charging energy and recovered energy account for relatively minor proportions, with their values fluctuating alongside changes in ISOC. This suggests that these two energy sources maintain generally stable ratios in the total energy composition and undergo staged

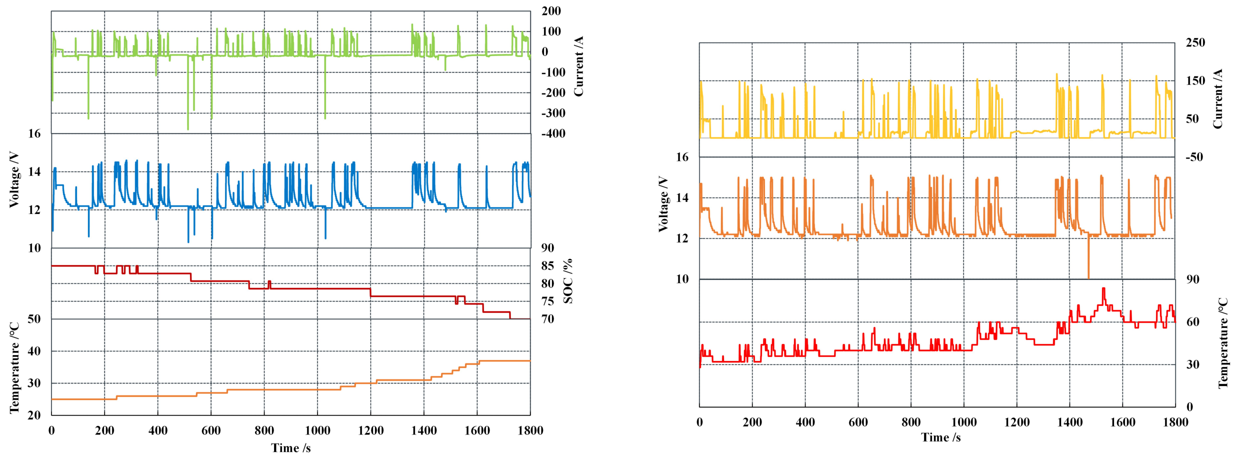

(a) Battery (b) Generator

Fig. 6. Instantaneous characteristics of battery and generator parameters at ISOC=85%.

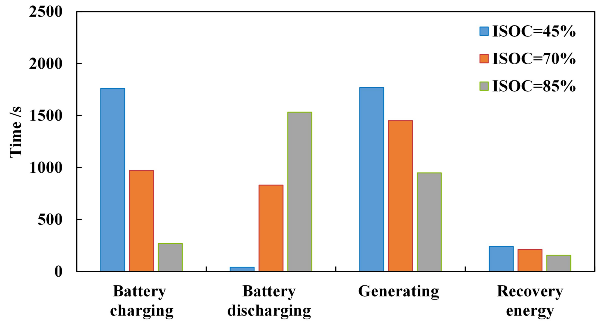

Fig. 7. Operation time of battery and generator at different ISOC

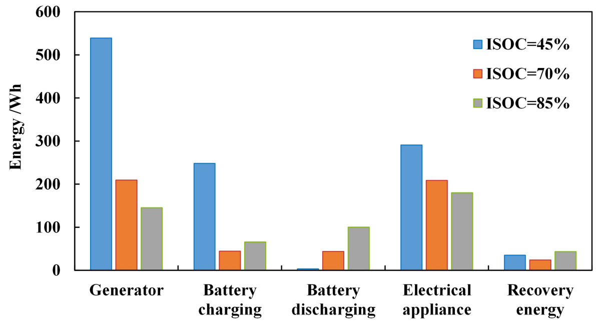

Fig. 9. Energy of battery, generator and onboard electrical appliances at different ISOC

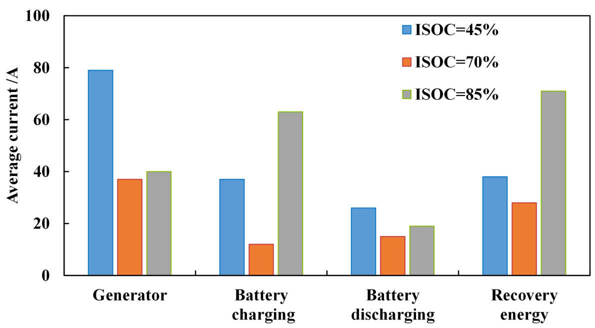

Fig. 8. Average current of battery and generator at different ISOC

changes modulated by the ISOC level. Specifically, a low ISOC leads to a higher proportion of charging energy due to the increased demand for battery replenishment. In contrast, a high ISOC lowers the need for charging, resulting in a lower share of charging energy.

Table 4. Energy percentage under different ISOC.

Table 4. Energy percentage under different ISOC.

Percentage /%	ISOC 45%	ISOC 70%	ISOC 85%
Generator	3.46	1.46	1.02
Battery charging	1.59	0.31	0.46
Battery discharging	0.02	0.31	0.70
Electrical appliance	1.87	1.46	1.26
Recovery energy	0.23	0.17	0.30

Fig. 10 displays vehicle fuel consumption under three ISOC conditions across the four WLTC speed phases (as detailed in Table 3) and throughout the entire WLTC cycle. It is evident that, ISOC exerts a significant influence on the overall vehicle fuel consumption. At high ISOC levels (70% and 85%), WLTC fuel consumption is reduced by 8.1% and 8.5%, respectively, in comparison to the 45% ISOC condition. The primary reason is that the WLTC cycle encompasses seven engine start–stop phases. However, at the ISOC of 45%, the intelligent start–stop function was deactivated, and only reactivated when the battery SOC exceeds 60%. Consequently, only one engine start-stop event occurred during the test. During the initial 6 start-stop phases (totaling 223 seconds) of the WLTC, the engine remained idling, leading to an increase in fuel consumption by 0.24 L/100km. Meanwhile, due to the low ISOC, the generator was compelled to operate longer to power the onboard electrical equipment, further increasing fuel consumption. When the ISOC values are 70% and 85% respectively, both surpassing the 60% start–stop activation threshold, all seven start–stop phases were executed in both cycles, resulting in similar fuel consumption levels. From the perspective of speed phases, fuel consumption at ISOC = 45% is the highest across all phases compared to higher ISOC levels. A plausible explanation is that with a low battery ISOC, the engine must intervene more frequently to maintain power output.

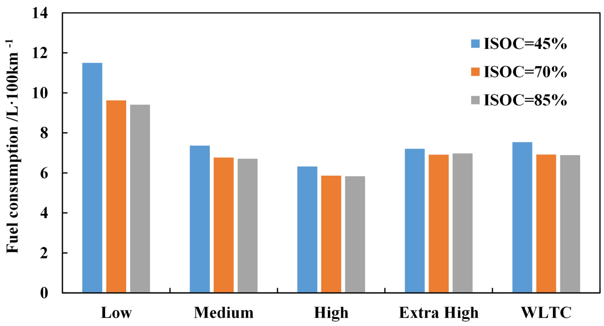

Fig. 10. Vehicle WLTC fuel consumption under different ISOC

During the low-speed phase, fuel consumption decreases markedly as ISOC increases. At 45% ISOC, fuel consumption stands at 11.5 L/100 km, and it drops by approximately 18.2% at 85% ISOC. In the medium-speed phase, fuel consumption shows a slight reduction as SOC increases. From 45% to 85% ISOC, fuel consumption decreases by 8.8%. Similarly, in the high-speed phase fuel consumption also decreases marginally with increasing SOC. As ISOC rises from 45% to 75% and 85%, fuel consumption decreases by approximately 8.9% and 7.8%, respectively. Regarding ultra-high speed phase, fuel consumption drops by 8.8% as ISOC increases from 45% to 85%.

A comparison of energy recovery efficiency under the three ISOC states is shown in Table 5, with three efficiency metrics defined. The first metric is the ratio of energy recovery time to total battery charging time, denoted as η_{time}. The second is the ratio of recovered energy to total battery charging capacity, labeled as η_{energy}. The third is the ratio of recovered energy to fuel consumption, referred to as η_{fuel}). It can be seen that ISOC significantly effects energy recovery efficiency. When the battery ISOC is at 85%, the proportion of energy recovery duration within the total charging duration reaches 58%. η_{time} drops to 18.9% when ISOC equals 70%, and further decreases to 13.6% at 45% ISOC. The energy recovery process constitutes only a part of the battery charging process. The ISOC value determines the variation in battery charging duration. Additionally, the proportion of energy recovery duration is also affected by the SOC threshold. Although the trend of η_{energy} is generally in line with that of η_{time}, it is also influenced by the operating current. At the 70% ISOC threshold, η_{energy} is substantially higher than η_{time} due to current effects. For the three ISOC levels, η_{fuel} is 0.8%, 0.6% and 1.1%, respectively, indicating that a higher ISOC is beneficial to improve the energy recovery efficiency.

Table 5. Energy recovery efficiency under different ISOC.

Efficiency	**ISOC**		
	45%	**70%**	**85%**
η_{time}	13.6%	18.9%	58.0%
η_{energy}	14.2%	35.1%	66.0%
η_{fuel}	0.8%	0.6%	1.1%

Based on the above results, two practical implications for control strategy design can be drawn. First, the battery charge-discharge threshold should not be set excessively low, and 70% appears to be an appropriate value. Second, if the battery SOC drops significantly (e.g., to 45%), the battery management system should trigger a maintenance or replacement alert.

This study was systematically conducted on an SUV platform under the WLTC cycle. Although the WLTC cycle covers a broad range of driving behaviors, real-world conditions, such as the Real Driving Emissions (RDE) cycle, merit further investigation. Therefore, the generalizability of the finding to other vehicle types and diverse driving scenarios remains constrained, which constitutes a clear limitation of this study. Nevertheless, the methodology framework established in this work provides a valuable reference for subsequent related research in the field. Future efforts will be dedicated to rigorously validating these findings across multiple vehicle platforms and under more complex driving cycles. Similarly, although the current study focuses on lead-acid batteries, the fundamental trend of ISOC effects on energy distribution is expected to be similar for lithium batteries, since both serve as onboard energy storage devices. Even so, the specific magnitude of the ISOC-induced impact remains to be studied and quantified. Regarding the aspect of battery aging, since long-term cycling aging causes SOC degradation, the three ISOC levels used in this study—85%, 70%, and 45%—can be reasonably regarded as representative conditions corresponding to mild, moderate, and severe aging states, respectively, which provides a rational basis for the experimental design of this work.

4. Conclusions

To systematically investigate the impact of battery ISOC on the vehicle's energy distribution, chassis dynamometer WLTC tests were conducted on a medium SUV equipped with start-stop and regenerative braking functions, with battery ISOC levels set at 45%, 70%, and 85%. Based on the experimental results, the following key conclusions are drawn:

i) **Battery ISOC significantly influences component operation modes and temperatures.** The ISOC level critically determines the operating modes of the battery and generator, thereby dominating the real-time energy distribution of the vehicle. Higher ISOC levels reduce the peak operating temperatures of both components, which is beneficial for maintaining operational efficiency and extending component lifespan.

ii) **ISOC determines component operating duration and energy flow direction.** At low ISOC (45%), the generator and battery operate predominantly in a continuous charging state. At the ISOC threshold (70%), the energy system approximates a dynamic equilibrium. And at high ISOC (85%), the generator's operating duration is markedly reduced, while the battery discharge period is extended, effectively lowering the engine load.

iii) **ISOC is crucial for fuel economy.** Operating at a low ISOC (45%) disables the intelligent start-stop function, leading to prolonged engine idling. Consequently, the WLTC cycle fuel consumption increases by approximately 8.1% and 8.5% compared to operating at ISOC levels of 70% and 85%, respectively.

iv) **High ISOC enhances energy recovery efficiency.** At an ISOC of 85%, energy recovery metrics such as the ratio of energy recovery time to total charging time and the ratio of recovered energy to total charging energy reach their optimal levels. This indicates that maintaining a high ISOC facilitates the maximization of regenerative braking energy utilization.

Acknowledgements

This study was funded by the Key Project of the Soft Science Research Program of Zhejiang Province under Grant No. 2026C25040.

References

[1] A. K. Agarwal, C. Mounaïm-Rousselle, P. Brequigny, A. Dhar, C. Hespel, C. Patel, D. K. Srivastava, G. Duraisamy, L. Le Moyne, N. Sharma, N. Labhasetwar, P. Singh, P. Das, P. K. Panigrahi, P. C. Shukla, P. Sakthivel, S. Mohan, S. Panigrahy, S. Sen, and H. Valera, (2025) *"Future of internal combustion engines using sustainable, scalable, and storable E-fuels and biofuels for decarbonizing transport and enabling advanced combustion technologies"* **Progress in Energy and Combustion Science *110***: 101236. DOI: https://doi.org/10.1016/j.pecs.2025.101236.

[2] A. O. Ali, O. Abdelrehim, M. M. Saafan, M. R. Elmarghany, and A. M. Hamed, (2025) *"Comprehensive review of battery management systems for electric vehicles: Thermal management, charging strategies, and emerging technologies"* **Journal of Power Sources *658***: 238269. DOI: https://doi.org/10.1016/j.jpowsour.2025.238269.

[3] P. Shrivastava, P. A. Naidu, S. Sharma, B. K. Panigrahi, and A. Garg, (2023) *"Review on technological advancement of lithium-ion battery states estimation methods for electric vehicle applications"* **Journal of Energy Storage *64***: 107159. DOI: https://doi.org/10.1016/j.est.2023.107159.

[4] C. Huang, Q. Shi, W. Ding, E. Q. Wu, and P. Mei, (2025) *"A Multirate-Fused State-of-Charge Estimation Scheme of Lithium-Ion Batteries for Electric Vehicles With Energy Harvesting Sensors"* **IEEE Transactions on Instrumentation and Measurement *74***: 1–11. DOI: 10.1109/TIM.2025.3547129.

[5] R. Guo and W. Shen, (2023) *"Lithium-Ion Battery State of Charge and State of Power Estimation Based on a Partial-Adaptive Fractional-Order Model in Electric Vehicles"* **IEEE Transactions on Industrial Electronics *70***(10): 10123–10133. DOI: 10.1109/TIE.2022.3220881.

[6] Q. Wang, C. Sun, and Y. Gu, (2023) *"Research on SOC estimation method of hybrid electric vehicles battery based on the grey wolf optimized particle filter"* **Computers and Electrical Engineering *110***: 108907. DOI: https://doi.org/10.1016/j.compeleceng.2023.108907.

[7] X. Lü, S. Li, X. He, C. Xie, S. He, Y. Xu, J. Fang, M. Zhang, and X. Yang, (2022) *"Hybrid electric vehicles: A review of energy management strategies based on model predictive control"* **Journal of Energy Storage** ***56***: 106112. DOI: https://doi.org/10.1016/j.est.2022.106112.

[8] J. J. Jui, M. A. Ahmad, M. I. Molla, and M. I. M. Rashid, (2024) *"Optimal energy management strategies for hybrid electric vehicles: A recent survey of machine learning approaches"* **Journal of Engineering Research** ***12***(3): 454–467. DOI: https://doi.org/10.1016/j.jer.2024.01.016.

[9] I. Jarraya, F. Masmoudi, M. H. Chabchoub, and H. Trabelsi, (2019) *"An online state of charge estimation for Lithium-ion and supercapacitor in hybrid electric drive vehicle"* **Journal of Energy Storage** ***26***: 100946. DOI: https://doi.org/10.1016/j.est.2019.100946.

[10] X. Zhao, L. Wang, Y. Zhou, B. Pan, R. Wang, L. Wang, and X. Yan, (2022) *"Energy management strategies for fuel cell hybrid electric vehicles: Classification, comparison, and outlook"* **Energy Conversion and Management** ***270***: 116179. DOI: https://doi.org/10.1016/j.enconman.2022.116179.

[11] A. S. Mohammed, S. M. Atnaw, A. O. Salau, and J. N. Eneh, (2023) *"Review of optimal sizing and power management strategies for fuel cell/battery/super capacitor hybrid electric vehicles"* **Energy Reports** ***9***: 2213–2228. DOI: https://doi.org/10.1016/j.egyr.2023.01.042.

[12] C. P. Sahwal, S. Sengupta, and T. Q. Dinh, (2024) *"Advanced Equivalent Consumption Minimization Strategy for Fuel Cell Hybrid Electric Vehicles"* **Journal of Cleaner Production** ***437***: 140366. DOI: https://doi.org/10.1016/j.jclepro.2023.140366.

[13] A. A. Mahajan and N. P. Mungle, (2025) *"Fuzzy Logic Based Power Distribution Strategy for Hybrid Fuel Cell Vehicle"* **Metallurgical and Materials Engineering** ***31***(3): 358–367. DOI: 10.63278/1385.

[14] M. Averbukh, B. Rivin, and J. Vinogradov. "On-Board Battery Condition Diagnostics Based on Mathematical Modeling of an Engine Starting System". In: *SAE World Congress & Exhibition*. SAE International, 2007. DOI: https://doi.org/10.4271/2007-01-1476.

[15] C. Armenta-Déu, (2024) *"Battery Management for Improved Performance in Hybrid Electric Vehicles"* **Vehicles** ***6***(2): 949–966. DOI: 10.3390/vehicles6020045.

[16] R. R. Kumar, C. Bharatiraja, K. Udhayakumar, S. Devakirubakaran, K. S. Sekar, and L. Mihet-Popa, (2023) *"Advances in Batteries, Battery Modeling, Battery Management System, Battery Thermal Management, SOC, SOH, and Charge/Discharge Characteristics in EV Applications"* **IEEE Access** ***11***: 105761–105809. DOI: 10.1109/ACCESS.2023.3318121.

[17] G. Vuylsteke, H. Wu, W. Moore, and D. Washington. "Impact of Battery Aging on the State of Charge-Open Circuit Voltage Relationship and Its Effects on Battery Capacity Estimation". In: *WCX SAE World Congress Experience*. SAE International, 2025. DOI: https://doi.org/10.4271/2025-01-8558.

[18] V. Duong, T. Thâm, W. Choi, and D.-W. Kim, (2016) *"State Estimation Technique for VRLA Batteries for Automotive Applications"* **Journal of Power Electronics** ***16***: 238–248. DOI: 10.6113/JPE.2016.16.1.238.

[19] J. Wishart, M. Shirk, T. Gray, and N. Fengler. "Quantifying the Effects of Idle-Stop Systems on Fuel Economy in Light-Duty Passenger Vehicles". In: *SAE 2012 World Congress & Exhibition*. SAE International, 2012. DOI: https://doi.org/10.4271/2012-01-0719.

[20] M. Debbou and F. Colet. "Inductive wireless power transfer for electric vehicle dynamic charging". In: *2016 IEEE PELS Workshop on Emerging Technologies: Wireless Power Transfer (WoW)*. 2016, 118–122. DOI: 10.1109/WoW.2016.7772077.

[21] C. Bharatiraja and G. Ramanathan. "A Hybridization of Photovoltaic and Battery Sources with Dual Input-Dual Output Converter for EV Charger". In: *Smart Grid Stability and Control*. Ed. by R. Krishan, D. R. Pullaguram, and S. R. Salkuti. Singapore: Springer Nature Singapore, 2025, 263–281. DOI: https://doi.org/10.1007/978-981-97-8634-3_18.

[22] M. Wang and T. Huang. "An Integrated Electric Energy Management System to Improve Fuel Economy". In: *Proceedings of the FISITA 2012 World Automotive Congress*. Berlin, Heidelberg: Springer Berlin Heidelberg, 2013, 115–122. DOI: https://doi.org/10.1007/978-3-642-33829-8_12.

[23] K. W. E. Cheng, B. P. Divakar, H. Wu, K. Ding, and H. F. Ho, (2011) *"Battery-Management System (BMS) and SOC Development for Electrical Vehicles"* **IEEE Transactions on Vehicular Technology** ***60***: 76–88. DOI: https://doi.org/10.1109/TVT.2010.2089647.

[24] S. Kim, K. Kim, J. Ha, S. Kwon, and Y. Seo, (2016) *"A Study about Impact of Battery SOC on Fuel Economy of Conventional Diesel Vehicle"* **Transactions of the Korean Society of Automotive Engineers *24***: 480–486. DOI: 10.7467/KSAE.2016.24.4.480.

[25] I. Cho and J. Lee, (2020) *"Characteristics of Battery SOC According to Drive Output and Battery Capacity of Parallel Hybrid Electric Vehicle"* **Applied Sciences *10***(8): DOI: 10.3390/app10082833.

[26] P. Ruetschi, (2004) *"Aging mechanisms and service life of lead–acid batteries"* **Journal of Power Sources *127***(1): 33–44. DOI: https://doi.org/10.1016/j.jpowsour.2003.09.052.

[27] S. Singirikonda and Y. P. Obulesu. "Advanced SOC and SOH Estimation Methods for EV Batteries—A Review". In: *Advances in Automation, Signal Processing, Instrumentation, and Control*. Ed. by V. L. N. Komanapalli, N. Sivakumaran, and S. Hampannavar. Singapore: Springer Nature Singapore, 2021, 1963–1977.

[28] Y. Wang, J. Tian, Z. Sun, L. Wang, R. Xu, M. Li, and Z. Chen, (2020) *"A comprehensive review of battery modeling and state estimation approaches for advanced battery management systems"* **Renewable and Sustainable Energy Reviews *131***: 110015. DOI: https://doi.org/10.1016/j.rser.2020.110015.

[29] J. S. Kim, J. W. Kim, J. H. Jeong, S. C. Jeong, and J. W. Lee, (2016) *"Effects of Initial SOC of 270-Volt Battery on Operating Performance of Gasoline Engine and Electric motor in a Parallel Hybrid Vehicle under IM240 Driving Cycle Mode"* **Advances in Automobile Engineering *2016***: 1–9. DOI: 10.4172/2167-7670.S1-008.

[30] United Nations. *Global technical regulation on worldwide harmonized light vehicles test procedure*. Tech. rep. ECE/TRANS/180/Add.15. Global Technical Regulation No. 15 (GTR 15) on Worldwide harmonized Light vehicles Test Procedures (WLTP), established in the Global Registry on 15 November 2017[reference:0]. United Nations, 2017.